Marine Geology 457 (2023) 107005

Contents lists available at ScienceDirect

Marine Geology

journal homepage: www.elsevier.com/locate/margo

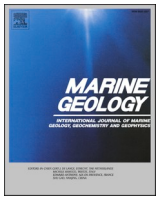

Research Article

Late Pleistocene chronostratigraphy and biostratigraphy of Mentelle Basin and its implications for global correlation

Maqsood Ur Rahman [a,b], Tao Jiang [a,b,*], Muhammad Sarim [c], Muhammad Hanif [d], Timothy T. Barrows [e], Yipan Hu [a,b]

[a] Hubei Key Laboratory of Marine Geological Resources, China University of Geosciences, Wuhan, China
[b] College of marine science and technology, China University of Geosciences, Wuhan, China
[c] State Key Laboratory of Continental Dynamics, Department of Geology, Northwest University, Xi'an, China
[d] National Centre of Excellence of Geology, University of Peshawar, Pakistan
[e] School of the Environment, Geography & Geosciences, University of Portsmouth, United Kingdom

ARTICLE INFO

Editor: Shu Gao

Keywords:
Nannofossils
Planktonic Foraminifera
Age Model
Indian Ocean
Global correlation

ABSTRACT

An accurate and high-resolution age model in marine sediments is essential for reconstructing past oceanographic and climate changes. The southeastern Indian Ocean is an important component of oceanographic circulation and global climate. However, the integrated biostratigraphy for the Late Pleistocene interval is not well known in the region. To address this issue, we constructed a new chronology for International Ocean Discovery Program (IODP) Hole U1516B in the Mentelle Basin, offshore southwestern Australia. We employ planktonic foraminifera $\delta^{18}O$ to construct an astronomically tuned age model for Hole U1516B. Biostratigraphic analysis was performed for Hole U1516B using planktonic foraminifera, nannofossils, radiolarian taxa and diatoms. Seven planktonic foraminifera events are recorded, including the PT1a and PT1b boundaries. Eight nannofossil events were recorded including the boundaries between CN14a, CN14b and CN15. The planktonic foraminifera datums marked in Hole U1516B are mostly synchronous with datums reported in the southern hemisphere but are diachronous with datums in the northern hemisphere. The nannofossil datums marked in Hole U1516B have a close affinity with globally reported datums but small inconsistencies are probably due to strong ecological control. The diatom events are inconsistent and only recorded in short intervals during interglacials and several key radiolarians taxa are absent.

1. Introduction

Glacial and interglacial climate events caused major palaeoceanographic changes during the Pleistocene. In particular, the last 800 ky have been characterized by strong warming in tropical and monsoon regions with intense cooling at higher latitudes (Ruddiman, 2006). Changes in ice volume are paralleled by fluctuation in proxies such as microfossil assemblages, stable isotopes and sediment characteristics in deep sea sedimentary sequences (Antonarakou et al., 2015; Guballa and Peleo-Alampay, 2020). In the Pleistocene, many periods are potential analogues to present climate, such as MIS 11 (Loutre and Berger, 2003), which may help understand future climatic changes (Guballa and Peleo-Alampay, 2020). To reconstruct the climatic and oceanographic changes in marine sediments, an accurate age model is essential (Antonarakou et al., 2019; Huybers and Wunsch, 2004; Lisiecki and Lisiecki, 2002; Ramsey, 2009a).

In recent decades, the Pleistocene nannofossil biostratigraphy has been greatly improved (Takayama and Sato, 1987; Matsuoka and Okada, 1989; Rio et al., 1990; Sato et al., 1991; Castradori, 1993; Raffi et al., 1993; Young, 1998; Hine and Weaver, 1998; de Kaenel et al., 1999; Flores et al., 1999, 2000, 2003; Raffi, 2002). The updated nannofossil biostratigraphy provides accurate and high-resolution datums for biochronology and global stratigraphic correlation. However, the Late Quaternary nannofossil biostratigraphy is less analysed in the Indian Ocean compared to the Atlantic Ocean, Pacific Ocean, and Mediterranean Sea (Supplementary Table S1). Similarly, planktonic foraminifera taxa provide first order biostratigraphic information (e.g., Wade et al., 2011). Globally, the planktonic foraminifera biostratigraphy in older ages is well developed (e.g., King et al., 2020; Lirer et al., 2019; Wade et al., 2011), but the biostratigraphic scheme is still

* Corresponding author at: Hubei Key Laboratory of Marine Geological Resources, China University of Geosciences, Wuhan, China.
E-mail address: taojiang@cug.edu.cn (T. Jiang).

https://doi.org/10.1016/j.margeo.2023.107005
Received 31 October 2022; Received in revised form 30 January 2023; Accepted 1 February 2023
Available online 9 February 2023

restricted to a few species (e.g., LO *Gr. tosaensis*) in the Late Pleistocene interval. In addition, the siliceous microfossils, Radiolaria and diatoms, have also been extensively used for biostratigraphy and palaeoceanography (e.g., Johnson et al., 1989; Moore Jr et al., 1993; Itaki, 2003; Motoyama and Nishimura, 2005; Cortese et al., 2012; Winter et al., 2012; Matsuzaki et al., 2014a, 2014b; Koizumi and Yamamoto, 2016; Kamikuri et al., 2017; Andrade et al., 2019).

Hole U1516B recovered during IODP Expedition 369 acquired a continuous record of the Upper Pleistocene in the Mentelle Basin, Southwestern Australia Huber et al. (2019a) (Fig.1). The Site U1516 preserved a unique record of the oceanography, climate and geological evolution of the Southeast Indian Ocean and offshore Southwestern Australia (e.g., Harry et al., 2020; Tagliaro et al., 2021, 2022). The region is characterized by important oceanographic currents and water masses e.g., Leeuwin Current (LC), Leeuwin Undercurrent (LUC), West Australian Current (WAC), Subtropical front (STF), Subtropical Water (STW), and South Indian Central Water (SICW). The U1516B can be used to study the complex paleoceanographic circulation offshore southwestern Australia (manuscript in preparation). Therefore, these cores offer the opportunity to build a high-resolution age model and provide a foundation for future paleoceanography studies.

In this study, we construct an age model for Hole U1516B using an astronomically tuned oxygen isotope record and radiocarbon dates. The age model is used to determine ages for biostratigraphic events in the planktonic foraminifera and nannofossil records. The biostratigraphic datums of the foraminiferal assemblages are globally correlated to both the southern and northern hemispheres. Finally, radiolarians and diatoms are also assessed for their biostratigraphic importance in the region.

2. Oceanographic setting around Southwestern Australia

Australia is a continent surrounded by surface and subsurface boundary currents flowing along the continental shelf and slope as components of the subtropical gyre circulation in the South Indian and South Pacific oceans (Domingues et al., 2007; Furue et al., 2017; Wijeratne et al., 2018). The transport of heat and mass flow towards the poles is important along both the east and west coasts of Australia. The Leeuwin Current System (LCS) is one of the important current systems in the eastern Indian Ocean (Fig. 1), which has three branches i.e., the Shelf Currents, the LC, and the LUC (Schloesser, 2014). The LC is characterized by the only southward flowing eastern boundary current in the Southern Hemisphere (Wijeratne et al., 2018). The ITF is the direct source of water for LC, which flows along a steric height gradient from the West Australian shelf towards the Southwest Cape of Australia (Domingues et al., 2007; Furue et al., 2017; Wijeratne et al., 2018). The central and southern South Indian Counter Current (SICC) is a major contributor (>60% inflows) to the LC in the west (Wijeratne et al., 2018). The warm and nutrient-poor LC suppress the coastal upwelling which results in the relatively oligotrophic nature of Western Australian waters (Koslow et al., 2008). The LUC has been noticed on the offshore edge of the LC on several occasions. The LUC typically exist at depth of 250 m to 500 m, flows northward and transports cool oxygen-rich waters north along the West Australian shelf (Domingues et al., 2007; Woo and Pattiaratchi, 2008; Schloesser, 2014; Wijeratne et al., 2018; Richardson et al., 2019).

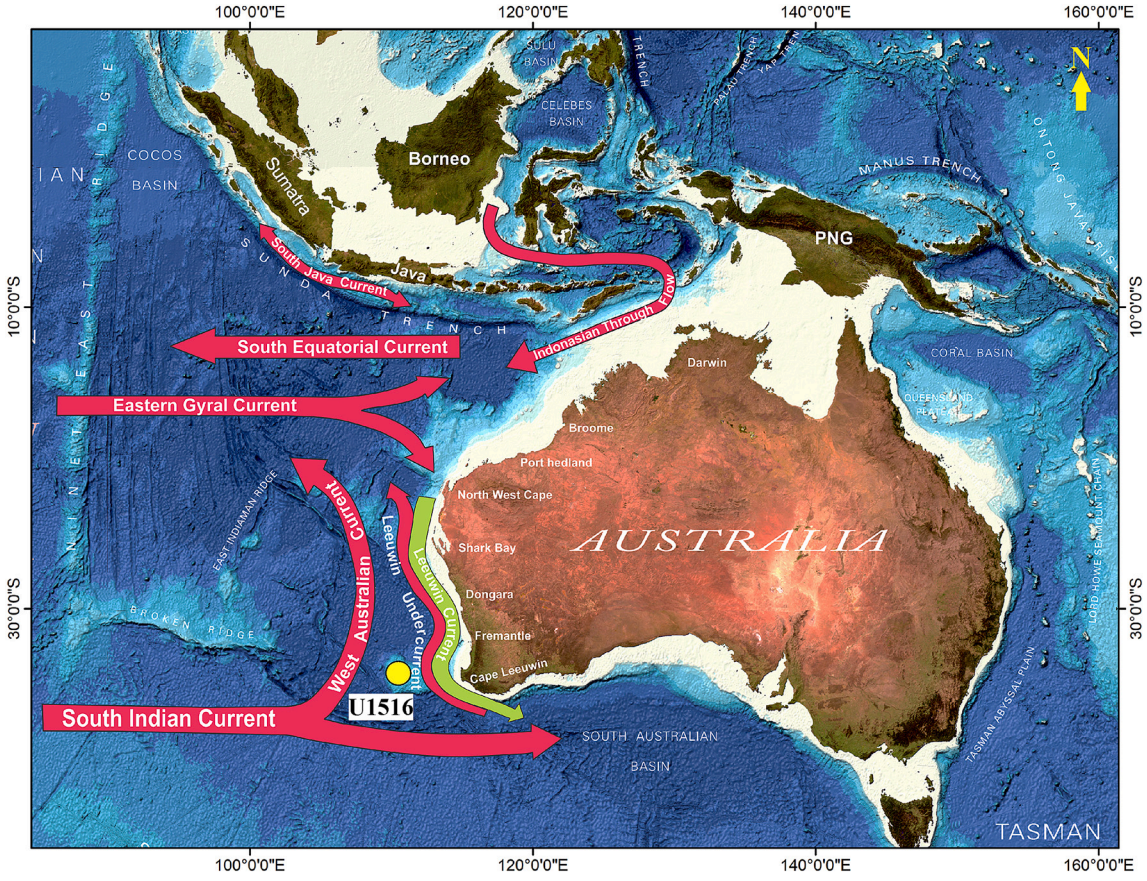

Fig. 1. The location of Site U1516 and the major oceanographic currents in the southeastern Indian Ocean, including Indonesian throughflow (ITF), Leeuwin Current (LC), Leeuwin Undercurrent (LUC), Eastern Gyral Current (EGC), South Equatorial Current (SEC), South Java Current (SJC)South Indian Current (SIC) and West Australian Current (WAC) (updated from Domingues et al., 2007).

3. Materials and methods

3.1. Core samples of IODP Hole U1516B

IODP Site U1516 was drilled during Expedition 369 in the Mentelle Basin (Fig. 1). Site U1516 comprises four holes (U1516A, B, C and D). Hole U1516A (34°20.9169′S, 112°47.9553′E) was drilled up to 223.6 m CSF-A and then the vessel was offset 20 m east to core Hole U1516B (34°20.9175′S, 112°47.9684′E). The Hole U1516B was drilled up to 16.2 m CSF-A with ~102% recovery (Huber et al., 2019a; Huber et al., 2019b). The cores were immediately sectioned into 30 cm whole rounds on the catwalk and sealed in light-proof bags with no further shipboard analysis. Since the cores from Hole U1516B are also cored and curated by IODP, the depth scheme of CSF-A can be used for this hole even though it was not included in the proceeding of IODP Expedition 369. The subsampling has been detected in the lab for biostratigraphic analysis, oxygen isotope analysis, and radiocarbon dating.

3.2. Oxygen isotope analysis

Oxygen isotope analysis was performed for Hole U1516B. The planktonic foraminiferal species *Globigerinoides* (*G*). *ruber* sensu stricto (s.s) (white) was selected for isotopic analysis from samples spaced about 10–13 cm apart while the initial few samples were taken at an interval of 4 cm. About 35–40 individuals of *G. ruber* s.s were picked from the >250 μm (250–355 μm) fraction. The tests of the foraminifera were carefully crushed into several fragments and were cleaned following the cleaning method of Barker et al. (2003). Stable oxygen isotope ratios of the planktonic foraminifera tests were measured on Thermo-Finnigan MAT-253 isotope ratio mass spectrometer with an online, automated carbonate preparation system (Kiel IV) at the State Key Laboratory of Geological Processes and Mineral Resources, China University of Geosciences, Wuhan. The values are reported per mil (‰) relative to Vienna Pee Dee Belemnite (VPDB) standard, calibrated by using GBW 04416 and GBW 04417 standards, along with a laboratory internal standard ISTB-1 (Supplementary Table DS1). Standards were run after every 10 samples and the standard deviation was <0.045% for $\delta^{18}O$.

3.3. Radiocarbon dating

The chronology for core top 0.75 m samples of Hole U1516B is based on seven accelerator mass spectrometry (AMS) radiocarbon (^{14}C) dates (Table 1). Planktonic foraminifera species *Globigerina inflata* were analysed at Beta Analytic Test Laboratory, United States of America (USA). AMS ^{14}C dates were calibrated using the MARINE20 calibration curve in BetaCal4.2 (Heaton et al., 2020; Ramsey, 2009b). The age is reported as radiocarbon years before present (BP), "present" = 1950 CE and is rounded to the nearest 10 years.

Table 1
Radiocarbon (^{14}C) ages of Hole U1516B upper 0.75 m CSF-A interval. (CI = confidence interval).

Samples	Depth CSF-A (m)	Lab identifier	Age BP (ky)	Age cal BP (ky) (95% CI)	$\delta^{13}C$ ‰
1H-1-J1-F-1	0.06–0.10	Beta-582,633	8.9 ± 20	8.2–7.8	0.9‰
1H-1-J1-F-2	0.13–0.16	Beta-594,965	9.6 ± 60	9.1–8.5	0.6‰
1H-1-J1-F-3	0.26–0.30	Beta-582,634	13.4 ± 40	14.2–13.7	0.9‰
1H-1-J2-F-1	0.30–0.33	Beta-594,967	19.7 ± 60	21.4–20.8	0.7‰
1H-1-J2-F-2	0.42–0.46	Beta-594,964	27.5 ± 120	19.1–28.6	0.8‰
1H-1-J3-F-1	0.60–0.63	Beta-594,968	32.6 ± 120	35.0–34.1	0.9‰
1H-1-J3-F-2	0.73–0.76	Beta-594,966	34.7 ± 230	37.7–36.7	0.9‰

3.4. Age model

The age model for Hole U1516B is based on the ^{14}C and $\delta^{18}O$ records. The $\delta^{18}O$ record of Hole U1516B was visually tuned to the $\delta^{18}O$ record *G. ruber* s.s with the astronomically tuned global benthic foraminifera $\delta^{18}O$ stack LR04 (Lisiecki and Raymo, 2005) (Figs. 3D and 5), using QAnalySeries (Kotov and Paelike, 2018; Paillard et al., 1996). Tuning a planktonic $\delta^{18}O$ to the benthic stack is justified on the grounds that the SST component of the record is small and therefore there is a good correspondence of oxygen isotope events between the two records. This approach has been used successfully elsewhere (Barrows et al., 2007) and the associated errors are unlikely to be significant beyond the last glacial cycle (Supplementary Fig. S1). 32 $\delta^{18}O$ tie points and seven ^{14}C ages (top 76 cm) were used for the tuning (Supplementary Table S2).

3.5. Biostratigraphy

Calcareous nannofossils, planktonic foraminifera, radiolarians and diatoms were identified for biostratigraphy of Hole U1516B. The samples were split into required aliquots (i.e., 0.5 g for nannofossils, 1 g for radiolarians and diatoms and 5 g for planktonic foraminifera) for analysis on the same depth levels. The sample preparation procedures followed are briefly discussed below.

3.5.1. Planktonic foraminifera

The core samples were dried overnight at 40^0C. 5 g of the dried samples were washed over a 74 μm sieve to obtain the planktonic foraminifera. The samples were then dried at room temperature. The fraction >150 μm was examined for diversity under a stereomicroscope. In each mixed sample, > 300 specimens were counted, excluding the broken and altered specimens (two rounds of analysis, overall >600 specimens). The entire samples were thoroughly examined above and below a biostratigraphic event/zone to ensure the presence or absence of species.

3.5.2. Calcareous nannofossils

Samples were prepared for nannofossils according to the method of Ma et al. (2019). For each sample, 0.5 g of dried bulk sample was disintegrated in 250 ml ultra HQ distilled water. The solution was kept in an ultrasonic bath for a short time. The weight of sediment, the amount of ultra HQ water, and the time in the ultrasonic bath remained the same for all samples. Then 330 μl of the well-mixed suspension was added to a coverslip using an automatic precision pipette and dried on a hot plate at a low temperature of 30–35 °C. After drying, the coverslip was mounted on a glass slide with Canada balsam. The sections were described at the State Key Laboratory of Biological Sciences, CUG, Wuhan by polarizing microscope. The sections were examined at 630× and 1000× resolution and photomicrographs were taken of each slide. For taxonomic nomenclature, the nomenclature described in Nannotax 3 (Young et al., 2018) was used. The species are well preserved and visible under the microscope.

3.5.3. Radiolaria and diatoms

For the analysis of Radiolaria and diatoms, 1 g of dry sediment was used. To remove the organic matter, the sediments were treated with 36% hydrogen peroxide (H_2O_2). After removing the organic matter, carbonates were removed with 30% hydrochloric acid (HCl). After keeping the sediments in HCl overnight, the HCl were washed three times (centrifuge method) with distilled water and the clean siliceous materials were kept in a test tube. The clean siliceous material was diluted in 3 ml of distilled water. The silica mixture of 330 μl was added to the glass coverslip and kept overnight to dry. After drying overnight, the coverslips were mounted to the slide with Canada balsam. The

sections were described at the State Key Laboratory for Biological Sciences, China University of Geosciences, Wuhan by polarizing microscope. The sections were studied at 200×, 400× and under plan light, while diatoms were studied with 630 x and 1000×.

4. Results

4.1. Orbitally tuned age model

The $\delta^{18}O$ record shows six complete glacial-interglacial cycles over the last 766 ky in Hole U1516B (Fig. 2) Some sections of the planktonic record do not show the full expected range of $\delta^{18}O$ values (e.g., MIS 9, 13) possibly due to under sampling. The age model of Hole U1516B is presented in Figs. 2 and 3. Sedimentation rates range between 1 and 4 cm/ky throughout the analysed cores increasing up to 6 cm/ky at top of the core probably due to less compacted sediments. Sedimentation rates show no obvious differences between glacial and interglacial cycles, but some cycles show a slight increase in interglacial cycles and vice versa (Fig. 3B).

4.2. Biostratigraphy

4.2.1. Planktonic foraminifera

Planktonic foraminifera are well preserved in the studied core samples of Hole U1516B. 38 species are recorded (Supplementary text S1), and 5 species (i.e., *Globorotalia* (*Gr*) *hessi, Gr. tosaensis, Gr. hirsuta, Globigerinoides* (*G*) *ruber* pink, *Globigerinella* (*Ge*) *calida*) show biostratigraphic datums. The first appearance datum (FAD) and last appearance datum (LAD) were recorded for each species (Table 2). The ages of the datums of planktonic foraminifera are mostly consistent with the calibrated biostratigraphic datums of Wade et al. (2011). Based on biostratigraphic datums, the core can be divided into two planktonic foraminiferal zones (i.e., PT1a and PT1b). The boundary between the zones is marked by the LAD of *Gr. tosaensis* at 610 ka. The lower part of the core (13.62–16.50 m CSF-A) is assigned to the PT1a zone, and the upper part of the core (0–13.60 m CSF-A) is assigned to PT1b (Fig. 4).

The FAD of *Gr. hessi* is recorded at 752 ka (16.03 m CSF-A) and LAD is recorded at 243.1 ka (4.33 m CSF-A). *Gr. hessi* is succeeded by zonal marker species *Gr. tosaensis* LAD at 610 ka. In PT1b the first event is marked by the FAD of *Gr. hirsuta* at 445 ka (9.70 m CSF-A). The first entry of the *G. ruber* pink is recorded at 399.2 ka (8.32 m CSF-A) and the LAD is recorded to be 124 ka (2.10 m CSF-A). The FAD of *Ge. calida* is recorded at 273.3 ka (5.40 m CSF-A). *Gr. flexuosa* is considered an important biostratigraphic marker species in the tropics with consistent FAD and LAD but is poorly preserved and rare in the studied samples. *G. conglobatus, Gr. scitula* and *Gc. puncticulata* disappeared during the last 100 ky but this might be because of environmental changes. These species have no biostratigraphic value regionally and globally (e.g., Wade et al., 2011).

4.2.2. Calcareous nannofossils

The nannofossils are well preserved throughout the studied core samples of Hole U1516B, and 24 taxa were identified (Supplementary text S2) (Fig. 5). FAD and LAD, first/last common occurrence (FCO/

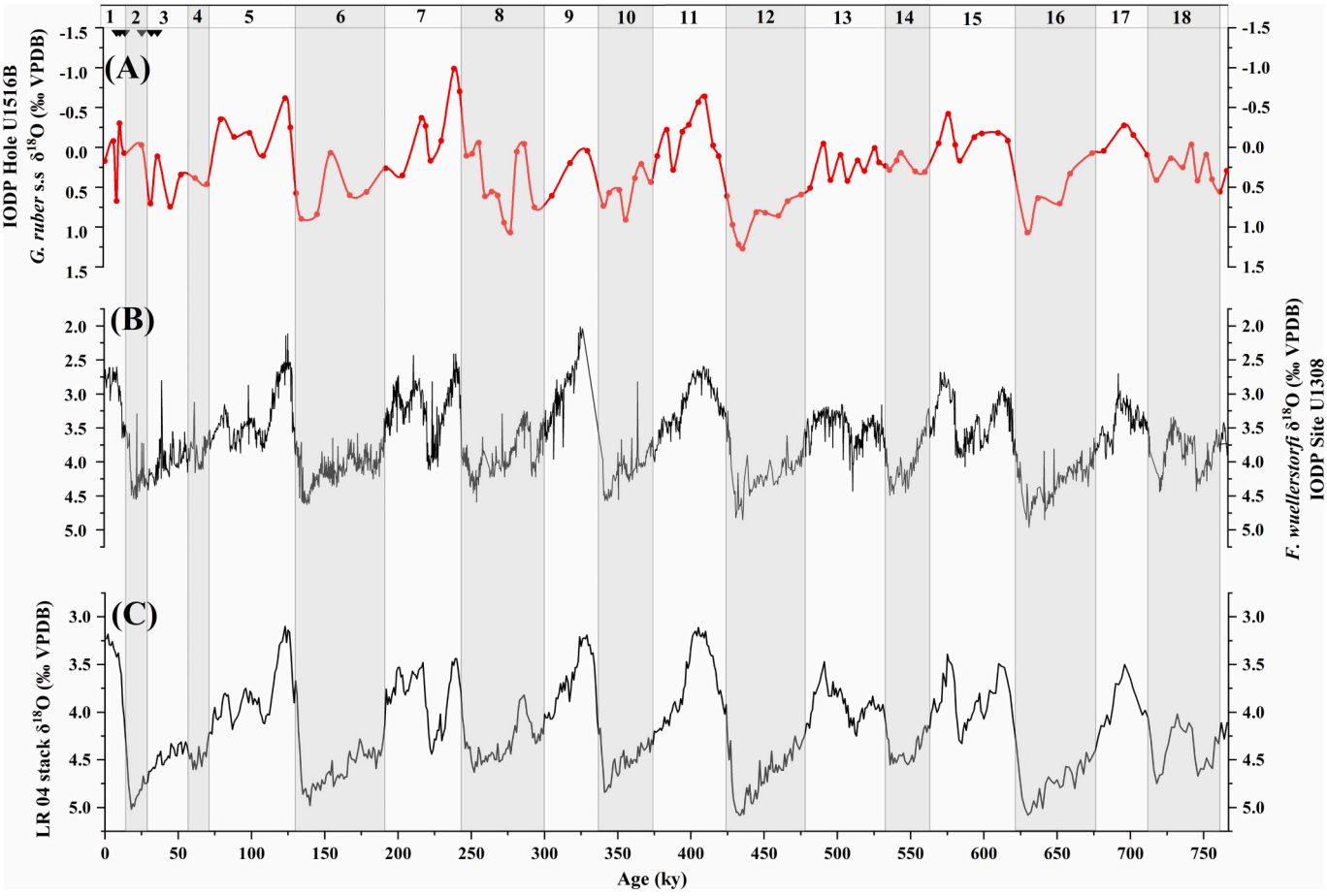

Fig. 2. $\delta^{18}O$ comparison of Hole U1516B with the MIS boundaries of Lisiecki and Raymo (2005). (A) The planktonic foraminifera *G. ruber* s.s. $\delta^{18}O$ (red line) from Hole U1516B, the small black triangles show the radiocarbon ages (B) middle latitude benthic foraminiferal *F. wuellerstorfi* $\delta^{18}O$ record from Site U1308 (Hodell et al., 2008), (C) the global benthic foraminiferal $\delta^{18}O$ stack LR04 (Lisiecki and Raymo, 2005). (For interpretation of the references to colour in this figure legend, the reader is referred to the web version of this article.)

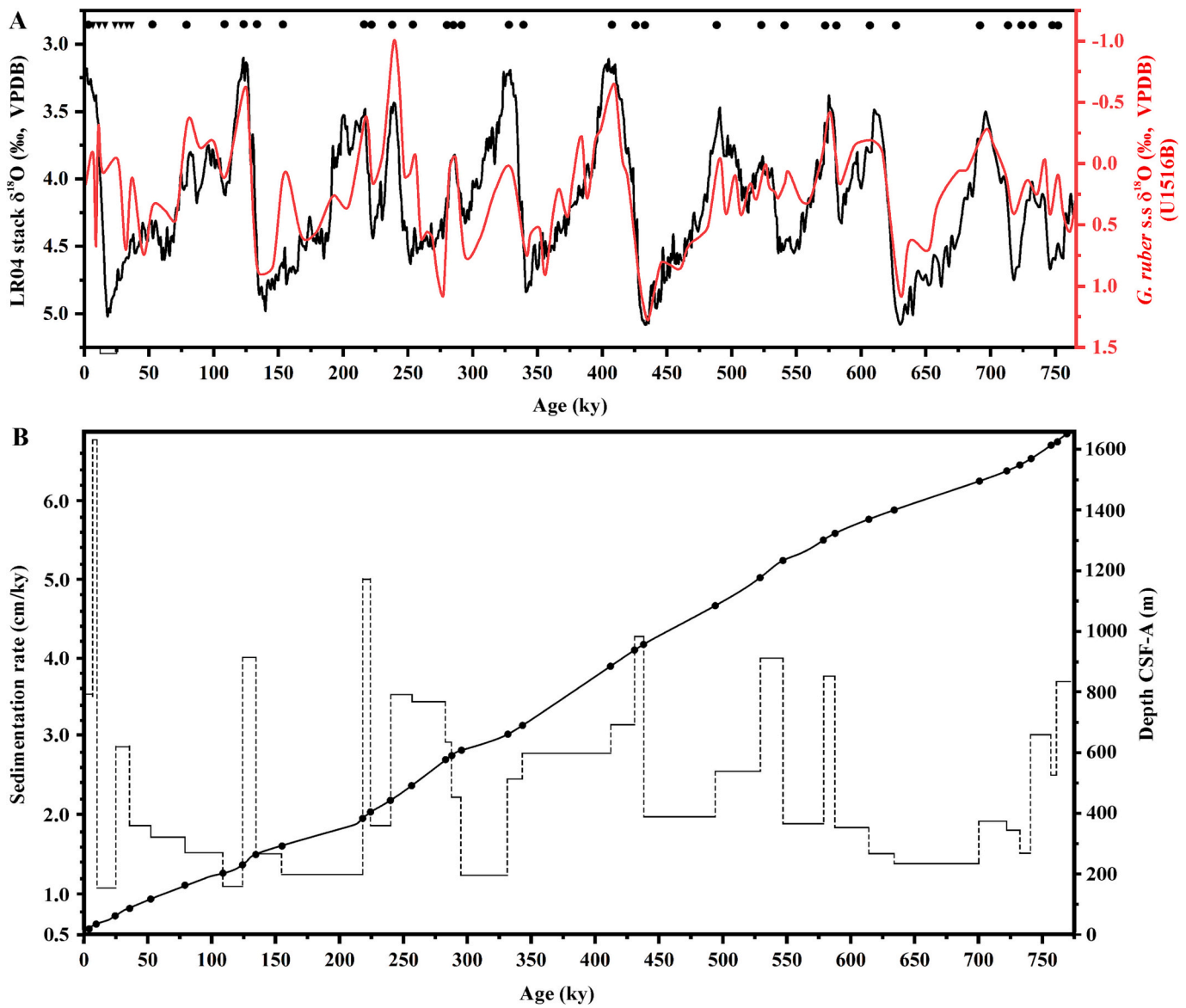

Fig. 3. Age model of Hole U1516B. (A) The planktonic foraminifera *G. ruber* s.s. $\delta^{18}O$ (red line) and the global benthic foraminiferal $\delta^{18}O$ stack LR04 (Lisiecki and Raymo, 2005) (black line), (black dots represent $\delta^{18}O$ tie point and black dots represent ^{14}C age tie point), (B) Depth-age model of sedimentary cores in Hole U1516B and sedimentation rate. (For interpretation of the references to colour in this figure legend, the reader is referred to the web version of this article.)

Table 2
Nannofossil events distinguished in Hole U1516B.

Planktonic events	Depth CSF-A (m)	Age (ka)
LAD of *G. ruber* pink	2.11	124
FAD of the *Globigerinella calida*	3.75	219.8
LAD of *Globorotalia hessi*	4.36	243.1
FE *G. ruber* pink	8.35	399.2
FAD of *Globorotalia hirsuta*	9.73	445
LAD of *Globorotalia tosaensis*	13.62	610
FAD of *Globorotalia hessi*	16.03	752

LCO) and highest abundance (acme zone) were determined (Fig. 6 and Table 3). The nannofossil datums recorded in this study have good consistency with the nannofossils biostratigraphical schemes of Martini (1971) and Okada and Bukry (1980). Only NN19 (only the upper part), NN20 and NN21 of Martini (1971), represent CN14a (only the upper part), CN14b and CN15 of Okada and Bukry (1980) are represented in the Hole U1516B. The boundary between NN19/NN20 and CN14a/CN14b is marked with the LAD of *Pseudoemiliania* (*P*) *lacunosa* at 425.2 ka (9.10 m FAD of *E. huxleyi* CSF-A). Similarly, the boundary between NN20/NN2 and CN14b/CN15 is marked by the FAD of *Emiliania* (*E*) *huxleyi* at 287 ka (5.83 m CSF-A). Besides the demarcation of the major biostratigraphic zones, a total of eight events were recorded in Hole U1516B (Table 3). Among the recorded events, *H. inversa* is the only nannofossil species with a complete zone that includes both FAD and LAD (Fig. 6).

4.2.3. Radiolarians

The diversity and abundance of radiolarian taxa in Hole U1516B are poor and several taxa that are normally common at low to middle latitudes are absent. Absent taxa include important biostratigraphical markers i.e., *Stylatractus universus, Collosphaera tuberos, Amphirhopalum ypsilon, Schizodiscus japonicus, Amphimelissa setosa,* and *Lychnocanoma sakaii*. Few species are consistently recorded whereas some are once or twice recorded (Supplementary text S3).

4.2.4. Diatoms

Diatom abundances were found not to be high enough in Hole

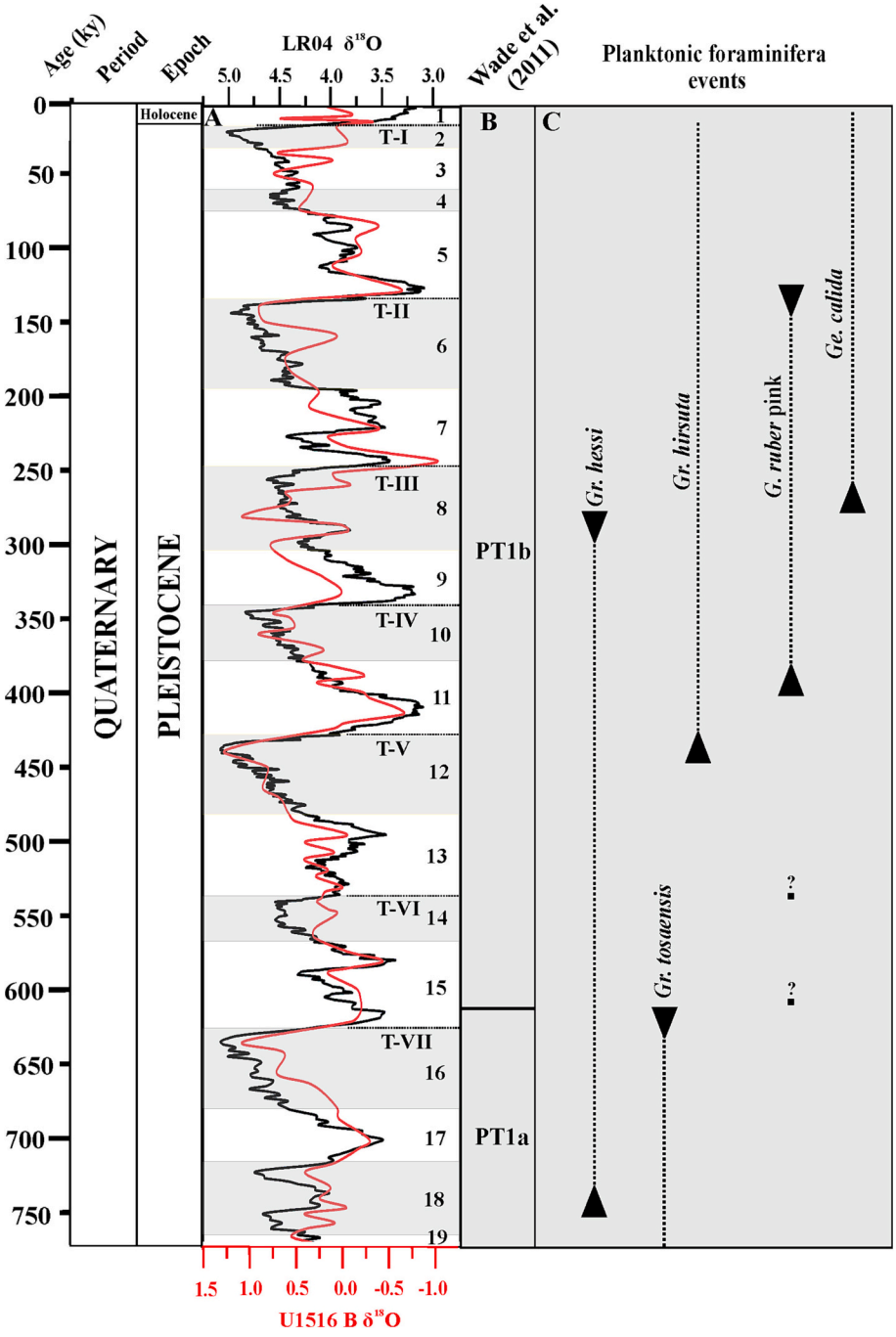

Fig. 4. Planktonic foraminifera biostratigraphy of Hole U1516B. (A) oxygen isotopes stratigraphy of Hole U1516B on the LR04 (Lisiecki and Raymo, 2005) age model and terminations (T-1–T-V), (B) Planktonic foraminifera biostratigraphic zones of Wade et al. (2011), (C) Planktonic foraminiferal events of this study,

U1516B to develop a regional zonation and were only identified at a generic level. The diatoms are restricted to the warm interglacials (Fig. 6). However, the occurrences of these diatoms can be considered as an event that might be reliable for regional age determination within Mentelle Basin.

Stellarima sp. was recorded at depth 0.60–0.63 m CSF-A in MIS 3 (32.1 ka). At depth of 3.3–3.33 m CSF-A in MIS 7 (192.5 ka) *Paralia sulcate* and *Cyclotella*? sp. were recorded. The occurrences of both genera/species are very close to the boundary between MIS 6/7. The occurrences of both species in the region can be used as a marker species for the demarcation of the boundary between MIS 6/7. *Cyclotella*? sp. is again recorded at depth 4.20–4.23 m CSF-A in MIS 7 (239 ka) which is also close to the boundary between MIS 7/8. *Cyclotella*? sp. is followed by *Thalassiosira* sp. at depth of 4.33–4.36 m CSF-A (243.1 ka) on the boundary between MIS 7/8. *Thalassiosira* sp. is further recorded at depths of 10.90–10.93, 13.00–13.13, 14.92–14.95 m CSF-A in MIS 13 (502.6 ka), MIS 15 (580–584 ka), and MIS 17 (702.2 ka). *Diploneis* sp. is observed at the depth of 10.90–10.93 m CSF-A in MIS 13 (502.6 ka).

5. Discussion

5.1. Global age framework of Planktonic foraminiferal

Taxonomy and biostratigraphy of planktonic foraminifera are the foundations for providing first-order relative age control in marine sediments, understanding open marine evolutionary dynamics, and

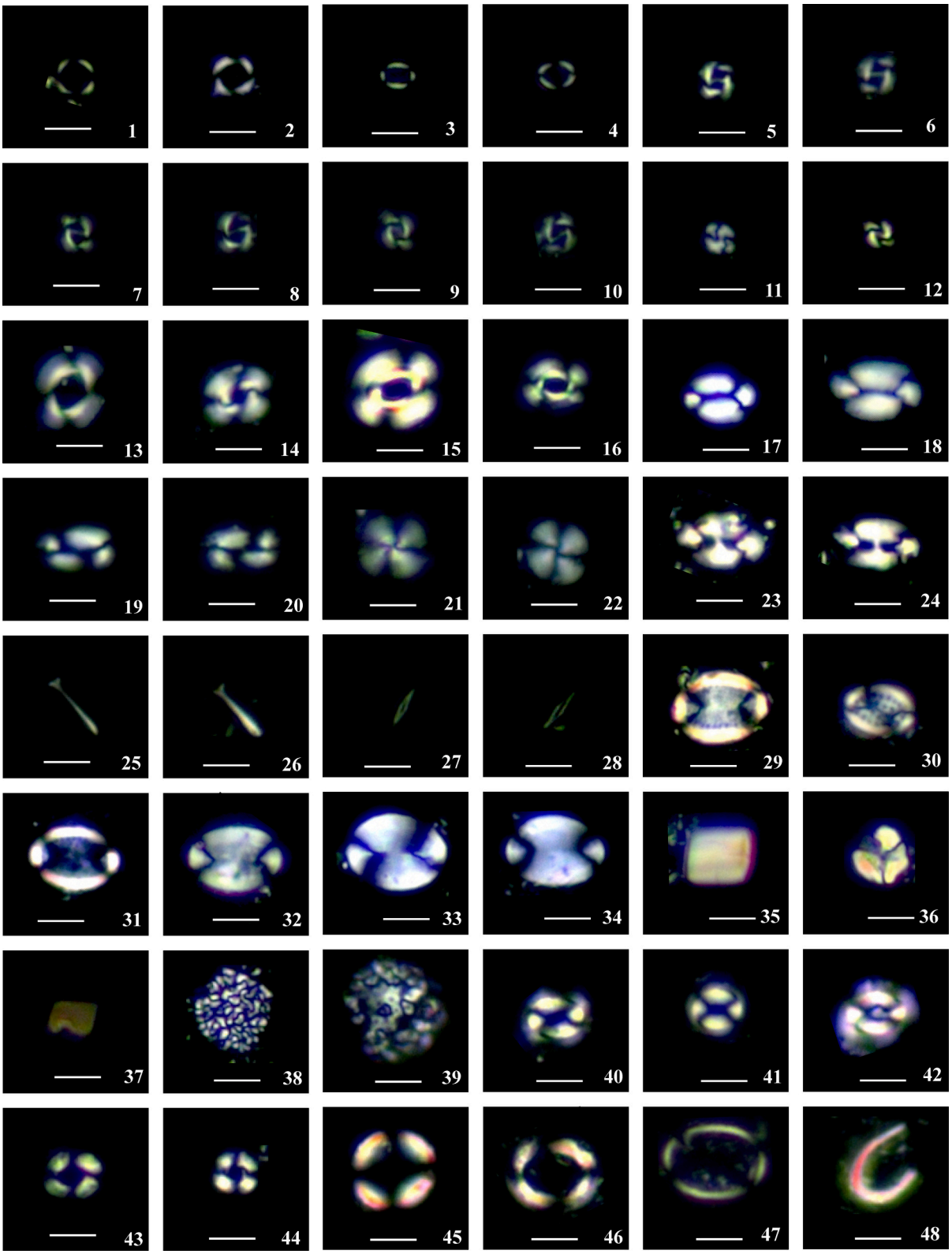

Fig. 5. Key nannofossils assemblages from Hole U1516B. 1–2 *Pseudoemiliania lacunose* (16.30 m CSF-A), 3–4 *Emiliania huxleyi* (1.60 m CSF-A), 5–6 *Gephyrocapsa omega* (1.60 m CSF-A), 7–8 *Gephyrocapsa oceanica* (1.60 m CSF-A), 9–10 *Gephyrocapsa muellerae* (1.60 m CSF-A), 11–12 *Gephyrocapsa caribbeanica* (1.60 m CSF-A), 13–14 *Reticulofenestra* sp. (16.30 m CSF-A), 15–16 *Reticulofenestra pseudoumbilicus*? (14.00 m CSF-A), 17–18 *Helicosphaera princei* (1.50 m CSF-A), 19–20 *Helicosphaera carteri* (1.50 m CSF-A), 21–22 *Calcidiscus leptoporus* (16.30 m CSF-A), 23–24 *Helicosphaera inversa* (9.40 m CSF-A), 25–26 *Rhabdosphaera claviger* (1.30 m CSF-A), 27–28 *Calciosolenia* sp. (1.30 m CSF-A), 29–31 *Pontosphaera discopora* (14.00 m CSF-A), 32–34 *Pontosphaera japonica* (1.60 m CSF-A), 35 *Gladiolithus flabellatus* (0.73 m CSF-A), 36 *Sphenolithus* sp. (0.73 m CSF-A), 37 *Florisphaera profunda* (0.73 m CSF-A), 38–39 *Algirosphaera robusta*? (0.73 m CSF-A), 40–41 *Coccolithus pelagicus* (11.00 m CSF-A), 42 *Coccolithus pelagicus* with bar (16.45 m CSF-A), 43–46 *Coccolithus* sp. (16.45, 14.00, 11.00 m CSF-A), 47 *Syracosphaera pulchra* (2.23 m CSF-A), 48 *Oolithotus* (16.45 m CSF-A).

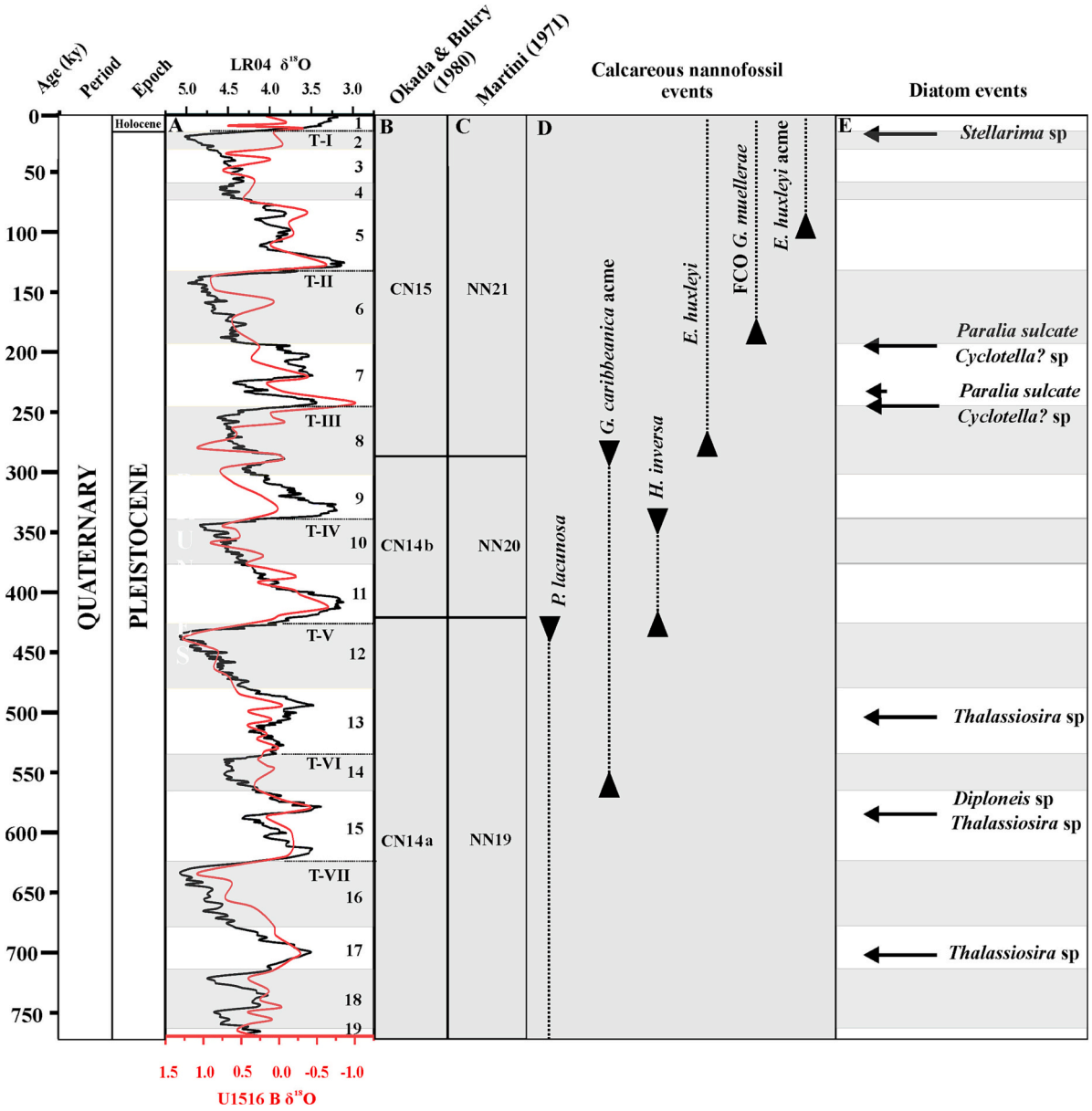

Fig. 6. Nannofossils biostratigraphy of Hole U1516B. (A) oxygen isotopes stratigraphy of Hole U1615B on the LR04 (Lisiecki and Raymo, 2005) age model and terminations (T-1–T-V), (B) nannofossils zones scheme of Okada and Bukry (1980), (C) nannofossils zones scheme of Martini (1971), (D) nannofossils events of this study, (E) The diatoms events recorded in Hole U1516B.

Table 3
Planktonic foraminiferal events are distinguished in Hole U1516B.

Nannofossil events	Depth CSF-A (m)	Age ka
E. huxleyi > Gephyrocapsa sp.	1.65	89.22
FCO of *G. muellerae*	3.31	192.5
LCO *G. caribbeanica*	4.95	260.1
FAD of *E. huxleyi*	5.86	287
LAD *H. inversa*	6.43	330
LAD *P. lacunosa*	9.13	425.2
FAD *H. inversa*	9.55	436
FCO *G. caribbeanica*	12.70	569.5

reconstructing ocean-climate history (Kennett and Srinivasan, 1983; King et al., 2020; Norris, 2000; Vats et al., 2020; Wade et al., 2011; Wei and Kennett, 1986). Planktonic foraminifera are globally important for biostratigraphy and correlations due to their evolutionary history (Sabba et al., 2022). The evolutionary characteristics of planktonic foraminifera can be considered ideal for biostratigraphic index fossils such as diversity (Fischer and Arthur, 1977; Loeblich and Tappan, 1987; Tappan and Loeblich Jr, 1973), morphology of lineage and species (Arnold et al., 1995; Cifelli, 1969; Malmgren and Kennett, 1981; Norris, 1996; Spencer-Cervato and Thierstein, 1997) and studying the dynamics of origins and extinctions of species (Thunell, 1981; Wei and Kennett, 1986) and biogeographic distribution through time (Parker et al., 1999). Therefore, they are widely utilized for biostratigraphy of Cretaceous and Cenozoic marine sediments and are a fundamental component of Cenozoic chronostratigraphy (Wade et al., 2011). The diachroneities in the planktonic foraminifera datums can be caused by various factors including the dispersal of species by ocean gyre (Darling et al., 2000), opening and closing of ocean gateways (Fenton, 2015; Haug and Tiedemann, 1998), ecology (Ding et al., 2006) and dissolution (Nguyen et al., 2009). In particular, the intensification of glacial-interglacial transitions during the Pleistocene strongly influenced the stratification

of surface waters and the marine environment as a whole (e.g., Crundwell et al., 2008; De Boer et al., 2010; Lisiecki and Raymo, 2005) These substantial environmental changes caused regional endemicity (Tsandev et al., 2008) which probably contributed to age diachronicities of planktonic foraminifera biostratigraphic events.

A total of seven biostratigraphic events were identified in U1516B, five of which are global and two are regional in nature (Table 4). The first event is marked with the FAD of *Gr. hessi* at 750 ka (Fig. 7). In tropical-subtropical regions, this event is globally synchronous at ~ 750 ka (Chaproniere et al., 1994; Wade et al., 2011) (Table 4). However, the LAD of *Gr. hessi* is geographically diachronous and categorized as a local/regional event due to age diachrony e.g., 400 ka (Aze et al., 2011), 80 ka (Bolli and Suva (1973) and 243 ka in Hole U1516B. The LAD of *Gr. tosaensis* occurs at the base of PT1b (610 ka) (e.g., Berggren et al., 1995b; Berggren et al., 1995a; Mix et al., 1995; Wade et al., 2011). The event is usually considered globally synchronous. However, the event is reported at 650 ka south of Australia (Li et al., 2003), as well as placed in the earlier zonation scheme of Berggren et al. (1995b, 1995a). The earlier extinction of *Gr. tosaensis* in the south of Australia could be caused by a colder climate during MIS 16 and possible northward migration of the Subtropical Front (STF) (e.g., Bard and Rickaby, 2009; Cartagena-Sierra et al., 2021). In the North Pacific Ocean, 293–586 ka is recorded by Lam and Leckie, 2020. The FAD of *Gr. hirsuta* marked another global event at 450 ka (Wade et al., 2011), consistent between the Indian Ocean (Hole U1516B; 445 ka) and the Southern Atlantic Ocean (Pujol and Duprat, 1983) (Fig. 7 and Table 4). The small age gap (~ 5 ky) is probably due to sampling resolution. Therefore, *Gr. hessi*, *Gr. tosaensis* and *Gr. hirsuta* likely signify globally synchronous events. These species belong to the Globorotalia genus which lives in the subsurface to deep water settings (e.g., Kucera, 2007; Schiebel and Hemleben, 2017), probably more resistant to local SST drop and other ecological changes compared to surface dwellers. Therefore, they show a global trend of evolution and extinction.

The FAD of the *Ge. calida* at 220 ka is potentially used as a biostratigraphic marker (Chaproniere et al., 1994; Berggren et al., 1995a; Wade et al., 2011). In this study, the FAD of *Ge. calida* occurs at 273.3 ka which is older than aforenamed studies. *Ge. calida* is an opportunistic species and commonly occurs in upwelling regions (e.g., Conan and Brummer, 2000; Retailleau et al., 2012; Schiebel et al., 2004; Schmuker, 2000), which means it responds to environmental changes and may have a diachronous FAD.

In the Indo-Pacific region, *G. ruber* pink at 120 ka is considered a reliable biostratigraphic marker in the Indo-Pacific region (Thompson et al., 1979; Wade et al., 2011; Jia et al., 2018), which is recorded at ~124 ka in this study. However, in the Indian Ocean (Hole U1516B) subevents of the *G. ruber* pink were found (Fig. 7), indicating environmental influence. In the Northern Pacific Ocean, the LAD of the species ranges between 238 and 327 ky (Lam and Leckie (2020).

From the above comparison, it is noticeable that the FAD and LAD of the reported species in Hole U1516B are quite similar to those from the tropical region (e.g., Wade et al., 2011), indicating the similar ecological conditions and flow of warm water from the tropical region through ITF and LC (e.g., Petrick et al., 2019). However, the planktonic foraminifera datums from Hole U1516B have obvious diachroneities with the subtropical Northern Pacific Ocean (Table 4). Besides environmental and ecological differences, the key factor that probably caused diachroneities is the dissolution factor, as high dissolution is recorded in the studied cores (Lam and Leckie, 2020). Dissolution can highly affect the planktonic foraminifera (Nguyen et al., 2009), which could cause the diachroneities in FAD and LAD of the planktonic foraminifera. The magnetostratigraphic age model of Lam and Leckie (2020) also seems to be affected by dissolution as very older ages were marked for younger species (Table 4). The planktonic foraminifera datums in the Indian Ocean (Hole U1516B) are synchronous with South Atlantic Ocean and Southern Pacific Ocean (Table 4). The similarities of planktonic foraminifera datums between the South Atlantic Ocean and Indian Ocean are probably due to the similar ecological conditions as both are characterized by the southward flow of warm surface water e.g., Agulhas Current (Gordon et al., 1987) and LC (Petrick et al., 2019). Similarly, the Southern Pacific Ocean (Lau Basin) situated in the tropical region provides similar surface water conditions as that of LC.

5.2. Global comparison of nannofossil events

The significance of nannofossils in the relative dating of marine sediments is because of their abundance and diversity, rapid evolution, preservation potential, and wide distribution in the marine environment (Raffi and Backman, 2022). Cenozoic nannofossils are considered one of the most powerful tools for biostratigraphic analysis and correlation in the marine realm (Agnini et al., 2017). The high-resolution chronostratigraphy coupled with nannofossil biostratigraphy allows for global correlation. Most of the nannofossil events reported in this study are synchronous with globally reported datums at least at the marine isotope stage (MIS) but some events show obvious diachroneities as shown in Table 4. The diachroneities in the nannofossil events are mainly caused by ecology and dissolution (e.g., Marsh, 2003; Thierstein et al., 1977). Similarly, the diversity and abundance of the nannofossil are highly controlled by the stratification of the water (e.g., Brand, 1994). Here we compare the identified nannofossil events in Hole U1516B with globally reported events (Fig. 8 and Table 4).

Based on the nannofossils encountered, three zones (NN19–21) are distinguished according to Martini (1971) and two zones (CN14–15)

Table 4
Global comparison of planktonic foraminifera and nannofossils events in the southern and northern hemispheres. The ages units are in kilo years ago (ka) while ages marked with a single asterisk (*) represent millions of years ago (Ma). In the southern hemisphere, the Indian Ocean represents the present study (Hole U1516B).

Events	Southern Hemisphere			Northern Hemisphere		
	Indian Ocean	Atlantic Ocean	Pacific Ocean	Atlantic Ocean	Pacific Ocean	Mediterranean Sea
LAD of *G. ruber* pink	124		120		238–327	
FAD of the *Ge. calida*	219.8				*3.087–0.254	
LAD of *Gr. hessi*	243.1			80		
FE *G. ruber* pink	399.2					
FAD of *Gr. hirsuta*	445	450			*1.123–0.673	
LAD of *Gr. tosaensis*	610				610–650, 293–586	
FAD of *Gr. hessi*	752		750			
E. huxleyi > Gephyrocapsa sp.	89.22	85		MIS4/5		55–81
FCO of *G. muellerae*	192.5	150	170			
LCO *G. caribbeanica*	260.1	280, 249				
FAD of *E. huxleyi*	287				290	274
LAD *H. inversa*	330	271, 250			540, 220	369
LAD *P. lacunosa*	425.2	447		390	460, 433, 440–436	424–406
FAD *H. inversa*	436			439		407
FCO *G. caribbeanica*	569.5	560, 540				

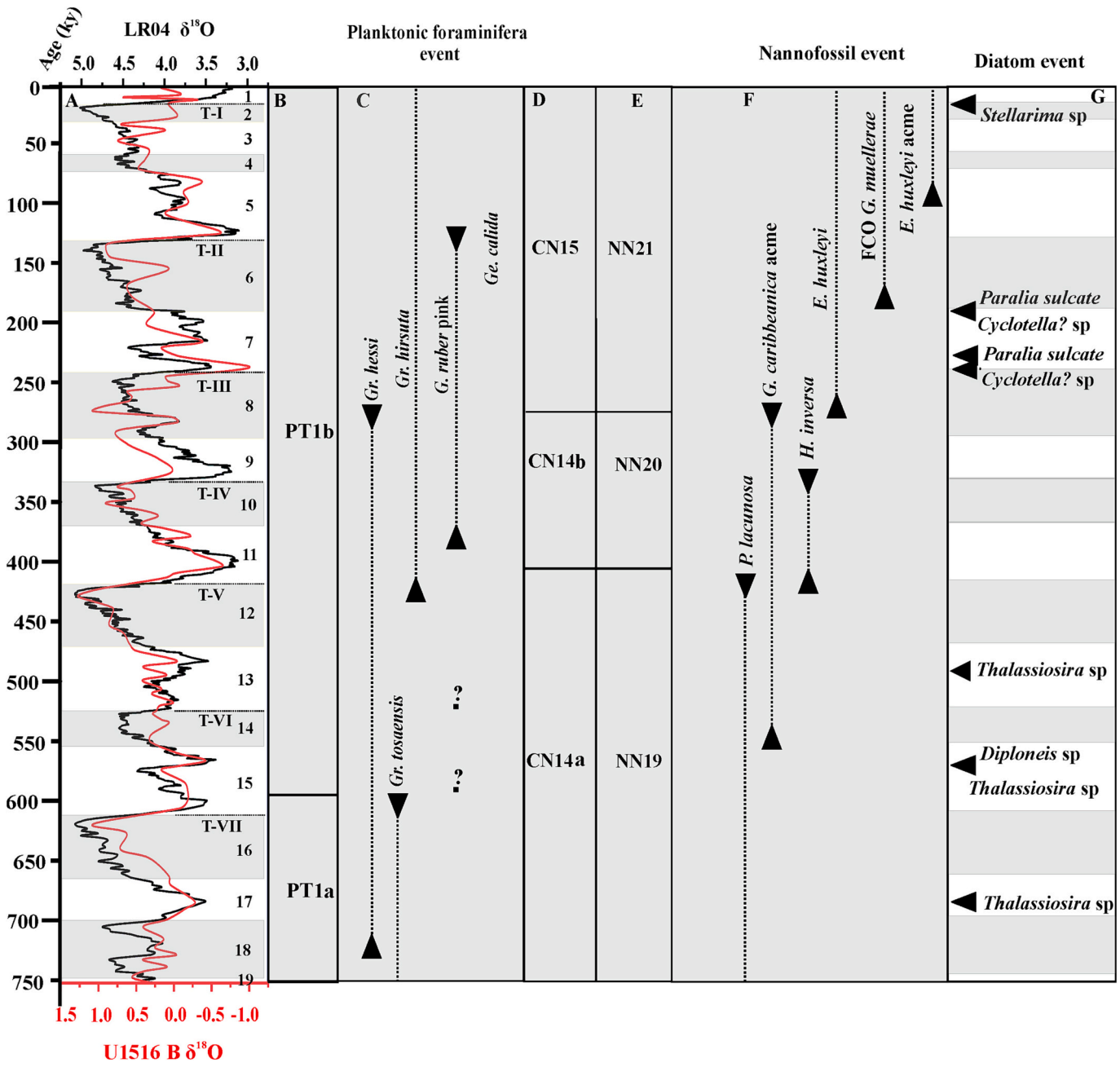

Fig. 7. (A) oxygen isotopes stratigraphy of Hole U1615B on the LR04 (Lisiecki and Raymo, 2005) age model and terminations (T-1–T-V), (B) planktonic foraminifera biostratigraphic zones of Wade et al. (2011), (C) planktonic foraminiferal events in Hole U1516B (D) nannofossils zones scheme of Okada and Bukry (1980), (E) nannofossils zones scheme of Martini (1971), (F) nannofossils events in Hole U1516B, (G) the diatoms events recorded in Hole U1516B.

according to the classification of Okada and Bukry (1980). The CN14 of Okada and Bukry (1980) is further divided into subzones i.e., CN14a and CN1b. Overall eight nannofossils events are recognized in the studied interval of U1516B and all are global in nature (Fig. 7 and Table 4). The boundary between NN19-NN20 and CN1a-CN1b is marked with the LAD of *P. lacunosa* at 425 ka (Fig. 7). Previously, the LAD of *P. lacunosa* is used as a boundary marker in the Mediterranean Sea, Atlantic and Pacific oceans in both hemispheres during 460–390 kyr (Berger et al., 1994; de Kaenel et al., 1999; Flores et al., 2003; Matsuzaki et al., 2015; Sato and Takayama, 1992; Takayama and Sato, 1987; Thierstein et al., 1977) (Table 4). The event is generally synchronous during MIS 12 with exceptions, but has significant age differences between different studies, because of the division of the event into two i.e., LADs of *P. lacunosa lacunosa* > 7 μm and elliptical *P. lacunosa* < 5 μm (e.g., Hay, 1970; Matsuoka and Okada, 1989). It is believed that the circular *P. lacunosa lacunosa* > 7 μm became extinct before the elliptical *P. lacunosa* < 5 μm (Hay, 1970), with a reported age gap of 30 ky in western Pacific Ocean Matsuoka and Okada (1989). In addition, the elliptical and circular *P. lacunosa* (< 5 μm) could not be distinguished in light microscopy here (de Kaenel et al., 1999).

The acme of *G. caribbeanica* is a well-established event of the Mid-Brunhes interval probably associated with globally changed climate (Baumann and Freitag, 2004; Bollmann et al., 1998; Lupi et al., 2012). In the studied interval of Hole U1516B, *G. caribbeanica* dominates other nannofossil species during the 569–260 ky (MIS15–8) interval (Fig. 7). In the South Atlantic Ocean, the *G. caribbeanica* acme is reported between 560 and 280 ky (Baumann and Freitag, 2004) and 540–249 ky (Flores et al., 2003). The acme of *G. caribbeanica* is mostly reported

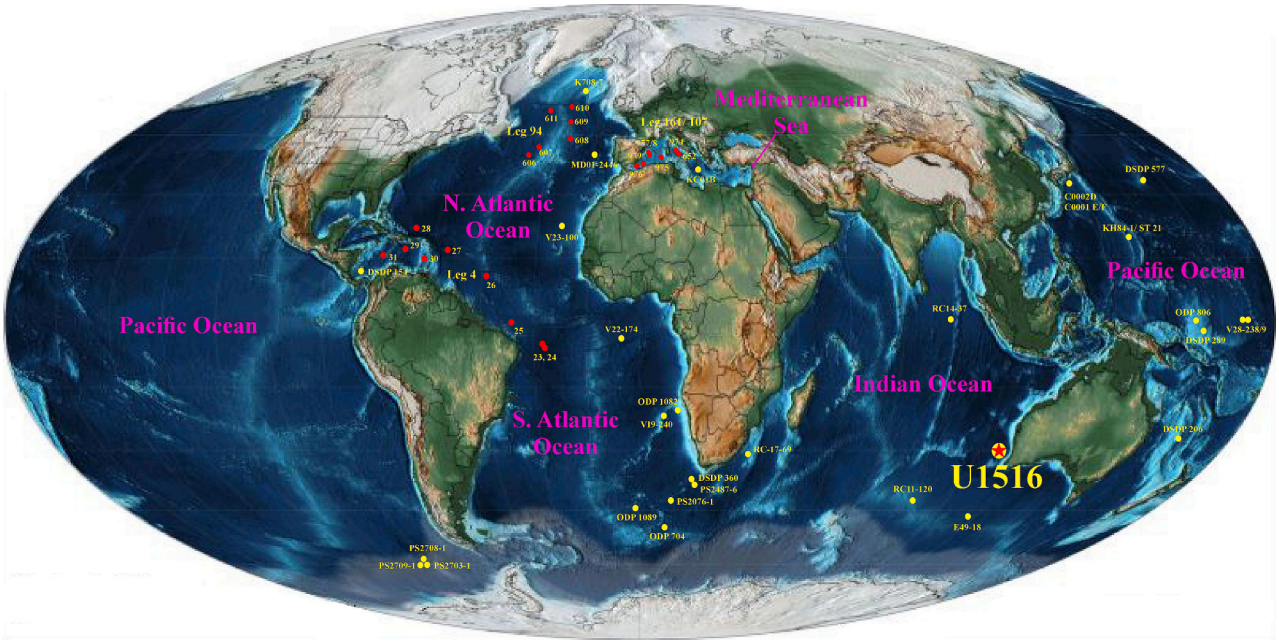

Fig. 8. Locations of Hole U1516B and other cores for global correlation. Positions of oceans and continents during the Pleistocene (modified from Scotese, 2014) with Hole U1516B and other cores for nannofossils correlation (See supplementary Table S1 for details).

during MIS 15–9, but local environmental changes causes minor age differences between studies. The FCO/LCO of the *G. caribbeanica* is synchronous between the Southeast Indian Ocean (Hole U1516B) and South Atlantic Ocean possibly due to close latitudinal position and ecological conditions (e.g., Baumann and Freitag, 2004; Flores et al., 2003; Gordon et al., 1987).

The *H. inversa* is the only nannofossil species which exhibits a complete zone in the Late Pleistocene (e.g., Maiorano et al., 2013). In this study, *H. inversa* occurred during the interval 436–330 ky (Fig. 7). Previously, the species is not very well documented and a few attempts recognize a narrow stratigraphic distribution during the Late Pleistocene (Takayama and Sato, 1987; Matsuoka and Okada, 1989; Marino et al., 2003; Maiorano et al., 2013). The species is reported in the Mediterranean Sea between 407 and 369 ky, and in the Atlantic Ocean between 439 and 160 ky (Maiorano et al., 2013; Sato et al., 1999; Sato and Takayama, 1992; Takayama and Sato, 1987). In the Pacific Ocean, the species is not recorded before 510 ka at mid-latitudes and 800 ka at low latitudes (Maiorano et al., 2013), whereas it disappeared (LAD) at 540 ka (Matsuoka and Okada, 1989) and 220 ka (Marino et al., 2003) respectively. The LAD and FAD of *H. inversa* are globally diachronous which is probably controlled by latitudinal changes in the stratification of the water, where the species arrived at ~800 ka in mid-latitudes and ~510 ka in low latitudes (Maiorano et al., 2013) (Table 4).

In Hole U1516B, the FCO of *G. muellerae* is recorded at 193 ka (MIS 6/7). The FCO of *G. muellerae* is previously recorded in the Agulhas Basin, South Atlantic and Southern oceans between 170 and 150 ky (MIS 6) (Flores et al., 2003; Flores et al., 2000; Flores et al., 1999). Available data from the Southern Hemisphere suggest that the FCO of *G. muellerae* is closely correlated and can be used for biostratigraphy. However, further studies at different locations are needed.

The last zone of the nannofossil biostratigraphic scheme of Martini (1971) (NN21) and Okada and Bukry (1980) (CN15) is marked with the FAD of *E. huxleyi* at 287 ka in U1516B (Fig. 7). Globally, this event is reported between 291 and 250 ky (Baumann and Freitag, 2004; de Kaenel et al., 1999; Flores et al., 2003; Matsuzaki et al., 2015; Thierstein et al., 1977) (Table 4). However, the generally accepted age is 290 ka (Raffi et al., 2006). The FAD of *E. huxleyi* is followed by the crossover (acme) of *E. huxleyi* on *Gephyrocapsa* populations (Gartner, 1977; de Kaenel et al., 1999). In Hole U1516B, the event is recorded at 89 ka (MIS 5), but the abundance is not high as recorded at other locations, possibly due to SST. In the North Atlantic Ocean, the event occurs at high latitudes during MIS 4 and at low latitudes during MIS 5 (Thierstein et al., 1977). The event is recorded in the Western Mediterranean Sea between 55 and 81 ka (MIS 4–5) and in the South Atlantic Ocean at 85 ka (MIS 5) (Flores et al., 2003). The event is diachronous because either the species is ecologically controlled or because of a relative reduction arising from dissolution (Thierstein et al., 1977).

6. Conclusions

IODP Hole U1516B preserves an excellent record of biostratigraphy based on nannofossils and planktonic foraminifera whereas the radiolarian taxa and diatoms are poorly preserved. This biostratigraphy can be used for further correlation with the sediments of the Pacific and Atlantic oceans and the Mediterranean Sea. The conclusions drawn from the current study are as follows:

- Seven planktonic foraminifera biostratigraphic events are identified, including the demarcation of the PT1b boundary.
- The planktonic foraminifera datums marked in Hole U1516B are mostly synchronous with datums previously marked in the southern hemisphere whereas diachronous with the northern hemisphere.
- Nannofossils are well preserved and show good diversity. Eight biostratigraphic events are identified including the *H. inversa* zone which is the only complete zone of the Late Pleistocene.
- The nannofossil datums marked in Hole U1516B have a close affinity with those globally reported but have small inconsistencies probably due to strong ecological control and dissolution factor.
- The radiolarian taxa and diatom are poorly preserved. The diatoms are restricted to specific intervals in interglacials whereas the radiolarian taxa are relatively consistent but key marker species are absent are rarely occurred.

Declaration of Competing Interest

The authors declare that they have no known competing financial interests or personal relationships that could have appeared to influence the work reported in this paper.

Data availability

The data used in the research article is available in the supplementary files on the journal website.

Acknowledgement

The author is extremely thankful to the IODP for providing the core samples. The author further acknowledges the efforts of IODP Expedition 369 scientists and technical staff members. This work is supported by the National Natural Science Foundation of China [No. 41976073 and 42276073]. The authors are grateful to Dr. Gabriel Tagliaro from University of São Paulo and an anonymous reviewer for their constructive comments.

Appendix A. Supplementary data

Supplementary data to this article can be found online at https://doi.org/10.1016/j.margeo.2023.107005.

References

Agnini, C., Monechi, S., Raffi, I., 2017. Calcareous nannofossil biostratigraphy: historical background and application in Cenozoic chronostratigraphy. Lethaia 50, 447–463.
Andrade, J., Legoinha, P., Stroynowski, Z., Abrantes, F., 2019. Morphology, biostratigraphy, and evolution of PliocenePleistocene diatoms Proboscia barboi. Geol. Acta 17, 1–17.
Antonarakou, A., Kontakiotis, G., Mortyn, P.G., Drinia, H., Sprovieri, M., Besiou, E., Tripsanas, E., 2015. Biotic and geochemical (δ18O, δ13C, Mg/Ca, Ba/Ca) responses of Globigerinoides ruber morphotypes to upper water column variations during the last deglaciation, Gulf of Mexico. Geochim. Cosmochim. Acta 170, 69–93.
Antonarakou, A., Kontakiotis, G., Karageorgis, A.P., Besiou, E., Zarkogiannis, S., Drinia, H., Mortyn, G.P., Tripsanas, E., 2019. Eco-biostratigraphic advances in late Quaternary geochronology and palaeoclimate: the marginal Gulf of Mexico analogue. Geol. Q 63.
Arnold, A.J., Kelly, D.C., Parker, W.C., 1995. Causality and Cope's rule: evidence from the planktonic foraminifera. J. Paleontol. 69, 203–210.
Aze, T., Ezard, T.H.G., Purvis, A., Coxall, H.K., Stewart, D.R.M., Wade, B.S., Pearson, P. N., 2011. A phylogeny of Cenozoic macroperforate planktonic foraminifera from fossil data. Biol. Rev. 86, 900–927.
Bard, E., Rickaby, R.E.M., 2009. Migration of the subtropical front as a modulator of glacial climate. Nature 460, 380–383.
Barker, S., Greaves, M., Elderfield, H., 2003. A study of cleaning procedures used for foraminiferal Mg/Ca paleothermometry. Geochem. Geophys. Geosyst. 4, 1–20. https://doi.org/10.1029/2003GC000559.
Barrows, T.T., Juggins, S., De Deckker, P., Calvo, E., Pelejero, C., 2007. Long-term sea surface temperature and climate change in the Australian–New Zealand region. Paleoceanography 22.
Baumann, K.-H., Freitag, T., 2004. Pleistocene fluctuations in the northern Benguela current system as revealed by coccolith assemblages. Mar. Micropaleontol. 52, 195–215.
Berger, W.H., Yasuda, M.K., Bickert, T., Wefer, G., Takayama, T., 1994. Quaternary time scale for the Ontong Java Plateau: Milankovitch template for ocean drilling program site 806. Geology 22, 463–467.
Berggren, W.A., Hilgen, F.J., Langereis, C.G., Kent, D.V., Obradovich, J.D., Raffi, I., Raymo, M.E., Shackleton, N.J., 1995a. Late Neogene chronology: new perspectives in high-resolution stratigraphy. Geol. Soc. Am. Bull. 107, 1272–1287.
Berggren, W.A., Kent, D.V., Swisher III, C.C., Aubry, M.-P., 1995b. A revised Cenozoic geochronology and chronostratigraphy. In: A., W., Berggren, D.V., Kent, M.-P., Aubry Hardenbol, J. (Eds.), Geochronology, Time Scales and Global Stratigraphic Correlation. SEPM Society for Sedimentary Geology, pp. 129–212. https://doi.org/10.2110/pec.95.04.0129.
Bolli, H.M., Suva, I.P., 1973. Oligocene to recent planktonic foraminifera and stratigraphy of the Leg 15 sites in the Caribbean Sea. In: Deep Sea Drilling Project, Initial Reports 15(1973). U.S. Govt. Printing Office, Washington, pp. 475–497. https://doi.org/10.2973/dsdp.proc.15.110.1973.
Bollmann, J., Baumann, K., Thierstein, H.R., 1998. Global dominance of Gephyrocapsa coccoliths in the late Pleistocene: selective dissolution, evolution, or global environmental change? Paleoceanography 13, 517–529.
Brand, L.E., 1994. Physiological ecology of marine coccolithophores. Coccolithophores 39–50.
Cartagena-Sierra, A., Berke, M.A., Robinson, R.S., Marcks, B., Castañeda, I.S., Starr, A., Hall, I.R., Hemming, S.R., LeVay, L.J., Party, E. 361 S, 2021. Latitudinal Migrations of the Subtropical Front at the Agulhas Plateau through the Mid-Pleistocene transition. Paleoceanogr. Paleoclimatol. 36, e2020PA004084.
Castradori, D., 1993. Calcareous nannofossil biostratigraphy and biochronology in eastern Mediterranean deep-sea cores. Riv. Ital. Paleontol. Stratigr. 99, 107–126.
Chaproniere, G.C.H., Styzen, M.J., Sager, W.W., Nishi, H., Quinterno, P.J., 1994. Late Neogene biostratigraphic and magnetostratigraphic synthesis, Leg 135. In: Proceedings of the Ocean Drilling Program. Scientific Results, pp. 857–877.
Cifelli, R., 1969. Radiation of Cenozoic planktonic foraminifera. Syst. Zool. 18, 154–168.
Conan, S.-H., Brummer, G.J.A., 2000. Fluxes of planktic foraminifera in response to monsoonal upwelling on the Somalia Basin margin. Deep Sea Res. Part II Top. Stud. Oceanogr 47, 2207–2227.
Cortese, G., Gersonde, R., Maschner, K., Medley, P., 2012. Glacial-interglacial size variability in the diatom Fragilariopsis kerguelensis: possible iron/dust controls? Paleoceanography 27, 1–14. https://doi.org/10.1029/2011PA002187.
Crundwell, M., Scott, G., Naish, T., Carter, L., 2008. Glacial–interglacial Ocean climate variability from planktonic foraminifera during the Mid-Pleistocene transition in the temperate Southwest Pacific, ODP Site 1123. Palaeogeogr. Palaeoclimatol. Palaeoecol. 260, 202–229.
Darling, K.F., Wade, C.M., Stewart, I.A., Kroon, D., Dingle, R., Brown, A.J.L., 2000. Molecular evidence for genetic mixing of Arctic and Antarctic subpolar populations of planktonic foraminifers. Nature 405, 43–47.
De Boer, B., Van de Wal, R.S.W., Bintanja, R., Lourens, L.J., Tuenter, E., 2010. Cenozoic global ice-volume and temperature simulations with 1-D ice-sheet models forced by benthic δ18O records. Ann. Glaciol. 51, 23–33.
Ding, X., Bassinot, F., Guichard, F., Li, Q.Y., Fang, N.Q., Labeyrie, L., Xin, R.C., Adisaputra, M.K., Hardjawidjaksana, K., 2006. Distribution and ecology of planktonic foraminifera from the seas around the Indonesian Archipelago. Mar. Micropaleontol. 58, 114–134.
Domingues, C.M., Maltrud, M.E., Wijffels, S.E., Church, J.A., Tomczak, M., 2007. Simulated Lagrangian pathways between the Leeuwin Current System and the upper-ocean circulation of the Southeast Indian Ocean. Deep Sea Res. Part II Top. Stud. Oceanogr. 54, 797–817.
Fenton, I., 2015. Environmental Controls on Planktonic Foraminiferal Diversity in Ancient and Modern Oceans. Imperial College London.
Fischer, A.G., Arthur, M.A., 1977. Secular Variations in the Pelagic Realm.
Flores, J.-A., Gersonde, R., Sierro, F.J., 1999. Pleistocene fluctuations in the Agulhas Current Retroflection based on the calcareous plankton record. Mar. Micropaleontol. 37, 1–22.
Flores, J.-A., Gersonde, R., Sierro, F.J., Niebler, H.-S., 2000. Southern Ocean Pleistocene calcareous nannofossil events: calibration with isotope and geomagnetic stratigraphies. Mar. Micropaleontol. 40, 377–402.
Flores, J.-A., Marino, M., Sierro, F.J., Hodell, D.A., Charles, C.D., 2003. Calcareous plankton dissolution pattern and coccolithophore assemblages during the last 600 kyr at ODP Site 1089 (Cape Basin, South Atlantic): paleoceanographic implications. Palaeogeogr. Palaeoclimatol. Palaeoecol. 196, 409–426.
Furue, R., Guerreiro, K., Phillips, H.E., McCreary Jr., J.P., Bindoff, N.L., 2017. On the Leeuwin Current System and its linkage to zonal flows in the South Indian Ocean as inferred from a gridded hydrography. J. Phys. Oceanogr. 47, 583–602.
Gartner, S., 1977. Calcareous nannofossil biostratigraphy and revised zonation of the Pleistocene. Mar. Micropaleontol. 2, 1–25.
Gordon, A.L., Lutjeharms, J.R.E., Gründlingh, M.L., 1987. Stratification and circulation at the Agulhas Retroflection. Deep Sea Res. Part A. Oceanogr. Res. Pap. 34, 565–599.
Guballa, J.D.S., Peleo-Alampay, A.M., 2020. Pleistocene Calcareous Nannofossil Biostratigraphy and Gephyrocapsid Occurrence in Site U1431D, IODP 349, South China Sea. Geosciences 10, 388. https://doi.org/10.3390/geosciences10100388.
Harry, D.L., Tejada, M.L.G., Lee, E.Y., Wolfgring, E., Wainman, C.C., Brumsack, H., Schnetger, B., Kimura, J., Riquier, L., Borissova, I., 2020. Evolution of the southwest Australian rifted continental margin during breakup of East Gondwana: results from International Ocean Discovery Program Expedition 369. Geochem. Geophys. Geosyst. 21, e2020GC009144.
Haug, G.H., Tiedemann, R., 1998. Effect of the formation of the Isthmus of Panama on Atlantic Ocean thermohaline circulation. Nature 393, 673–676.
Hay, W.W., 1970. Calcareous Nannofossils from Cores Recovered on Leg 4. Deep Sea Drill. Proj. Initial Rep. 4, 455–501. https://doi.org/10.2973/dsdp.proc.4.123.1970.
Heaton, T.J., Köhler, P., Butzin, M., Bard, E., Reimer, R.W., Austin, W.E.N., Ramsey, C.B., Grootes, P.M., Hughen, K.A., Kromer, B., 2020. Marine20—the marine radiocarbon age calibration curve (0–55,000 cal BP). Radiocarbon 62, 779–820.
Hine, N., Weaver, P.P.E., 1998. Calcareous nannofossil biostratigraphy, in: Quaternary. In: Bown, P.R. (Ed.), Dordrecht. Kluwer Academic Publishers, pp. 266–283.
Hodell, D.A., Channell, J.E.T., Curtis, J.H., Romero, O.E., Rohl, U., 2008. Oxygen and carbon isotopes of the benthic foraminifer Cibicoides wuellerstorfi of IODP Site 303-U1308. Suppl. To Hodell, DA al. Onset "Hudson Strait" Heinrich events East. North Atl. End middle Pleistocene Transit. (~640 ka)? Paleoceanogr 23 (4), PA4218 doi: 10.1029/2008PA001591. https://doi.org/10.1594/PANGAEA.831735.
Huber, B.T., Hobbs, R.W., Bogus, K.A., Batenburg, S.J., Brumsack, H.-J., do Monte Guerra, R., Edgar, K.M., Edvardsen, T., Garcia Tejada, M.L., Harry, D.L., Hasegawa, T., Haynes, S.J., Jiang, T., Jones, M.M., Kuroda, J., Lee, E.Y., Li, Y.-X., MacLeod, K.G., Maritati, A., Martinez, M., O'Connor, L.K., Petrizzo, M.R., Quan, T. M., Richter, C., Riquier, L., Tagliaro, G.T., Wainman, C.C., Watkins, D.K., White, L.T., Wolfgring, E., Xu, Z., 2019a. U1516. In: International Ocean Discovery Program. https://doi.org/10.14379/iodp.proc.369.102.2019.
Huber, B.T., Hobbs, R.W., Bogus, K.A., Batenburg, S.J., Brumsack, H.-J., Monte, D., Guerra, R.E., Edgar, K.M., Edvardsen, T., Harry, D.L., Hasegawa, T., Haynes, S.J., Jiang, T., Jones, M.M., Kuroda, J., Lee, E.Y., Li, Y.-X., MacLeod, K.G., Maritati, A., Martinez, M., O'Connor, L.K., Petrizzo, M.R., Quan, T.M., Richter, C., Riquier, L., Tagliaro, G.T., Garcia Tejada, M.L., Wainman, C.C., Watkins, D.K., White, L.T., Wolfgring, E., Xu, Z., 2019b. Australia cretaceous climate and Tectonics. Proc. Int. Ocean Discov. Progr. 369 https://doi.org/10.14379/iodp.proc.369.107.2019 2 Expedition 369 Scientists' aff.

Huybers, P., Wunsch, C., 2004. A depth-derived Pleistocene age model: uncertainty estimates, sedimentation variability, and nonlinear climate change. Paleoceanography 19.
Itaki, T., 2003. Depth-related radiolarian assemblage in the water-column and surface sediments of the Japan Sea. Mar. Micropaleontol. 47, 253–270.
Jia, Q., Li, T., Xiong, Z., Steinke, S., Jiang, F., Chang, F., Qin, B., 2018. Hydrological variability in the western tropical Pacific over the past 700 kyr and its linkage to Northern Hemisphere climatic change. Palaeogeogr. Palaeoclimatol. Palaeoecol. 493, 44–54.
Johnson, D.A., Schneider, D.A., Nigrini, C.A., Caulet, J.P., Kent, D.V., 1989. Pliocene-Pleistocene radiolarian events and magnetostratigraphic calibrations for the tropical Indian Ocean. Mar. Micropaleontol. 14, 33–66.
de Kaenel, E., Siesser, W.G., Murat, A., Zahn, R., 1999. Pleistocene Calcareous Nannofossil Biostratigraphy and the Western Mediterranean Sapropels, Sites 974 to 977 and 979, in: Proceedings of the Ocean Drilling Program. Scientific Results. Ocean Drilling Program College Station, Texas, USA, pp. 159–183.
Kamikuri, S.-I., Itaki, T., Motoyama, I., Matsuzaki, K.M., 2017. Radiolarian biostratigraphy from middle Miocene to late Pleistocene in the Japan Sea. Paleontol. Res. 21, 397–421.
Kennett, J.P., Srinivasan, M.S., 1983. Neogene Planktonic Foraminifera, A phylogenetic atlas. Hutchinson Ross Publishing Company, London.
King, D.J., Wade, B.S., Liska, R.D., Miller, C.G., 2020. A review of the importance of the Caribbean region in Oligo-Miocene low latitude planktonic foraminiferal biostratigraphy and the implications for modern biogeochronological schemes. Earth-Science Rev. 202, 102968.
Koizumi, I., Yamamoto, H., 2016. Diatom records in the Quaternary marine sequences around the Japanese Islands. Quat. Int. 397, 436–447.
Koslow, J.A., Pesant, S., Feng, M., Pearce, A., Fearns, P., Moore, T., Matear, R., Waite, A., 2008. The effect of the Leeuwin current on phytoplankton biomass and production off Southwestern Australia. J. Geophys. Res. Ocean. 113, C07050. https://doi.org/10.1029/2007JC004102.
Kotov, S., Paelike, H., 2018. QAnalySeries-a cross-platform time series tuning and analysis tool. In: AGU Fall Meeting Abstracts pp. PP53D-1230.
Kucera, M., 2007. Chapter six planktonic foraminifera as tracers of past oceanic environments. Dev. Mar. Geol. 1, 213–262.
Lam, A.R., Leckie, R.M., 2020. Subtropical to temperate late Neogene to Quaternary planktic foraminiferal biostratigraphy across the Kuroshio Current Extension, Shatsky rise, Northwest Pacific Ocean. PLoS One 15, e0234351.
Li, Q., McGowran, B., Brunner, C.A., 2003. Neogene planktonic foraminiferal biostratigraphy of sites 1126, 1128, 1130, 1132 and 1134, ODP Leg 182, Great Australian Bight. In: Proc. ODP Sci. Results, pp. 1–66.
Lirer, F., Foresi, L.M., Iaccarino, S.M., Salvatorini, G., Turco, E., Cosentino, C., Sierro, F. J., Caruso, A., 2019. Mediterranean Neogene planktonic foraminifer biozonation and biochronology. Earth-Science Rev. 196, 102869.
Lisiecki, L.E., Lisiecki, P.A., 2002. Application of dynamic programming to the correlation of paleoclimate records. Paleoceanography 17, 1.
Lisiecki, L.E., Raymo, M.E., 2005. A Pliocene-Pleistocene stack of 57 globally distributed benthic δ18O records. Paleoceanography 20, 1–17. https://doi.org/10.1029/2004PA001071.
Loeblich, A.R., Tappan, H., 1987. Foraminiferal Genera and their Classification. Van Reinhold Company, New York 2.
Loutre, M.-F., Berger, A., 2003. Marine Isotope Stage 11 as an analogue for the present interglacial. Glob. Planet. Chang. 36, 209–217.
Lupi, C., Bordiga, M., Cobianchi, M., 2012. Gephyrocapsa occurrence during the Middle Pleistocene transition in the Northern Pacific Ocean (Shatsky rise). Geobios 45, 209–217.
Ma, R., Liu, C., Li, Q., Jin, X., 2019. Calcareous nannofossil changes in response to the spreading of the South China Sea basin during Eocene-Oligocene. J. Asian Earth Sci. 184, 103963.
Maiorano, P., Tarantino, F., Marino, M., Girone, A., 2013. A paleoecological and paleobiogeographic evaluation of Helicosphaera inversa (Gartner) Theodoridis and the diachrony of its first occurrence. Mar. Micropaleontol. 104, 14–24.
Malmgren, B.A., Kennett, J.P., 1981. Phyletic gradualism in a late Cenozoic planktonic foraminiferal lineage; DSDP Site 284, Southwest Pacific. Paleobiology 7, 230–240.
Marino, M., Maiorano, P., Monechi, S., 2003. Quantitative Pleistocene calcareous nannofossil biostratigraphy of Leg 86, Site 577 (Shatsky rise, NW Pacific Ocean). J. Nannoplankt. Res. 25, 25–37.
Marsh, M.E., 2003. Regulation of CaCO3 formation in coccolithophores. Comp. Biochem. Physiol. Part B Biochem. Mol. Biol 136, 743–754.
Martini, E., 1971. Standard Tertiary and Quaternary Calcareous Nannoplankton Zonation. In: Proc. II Planktonic Conference, Roma 1970, Roma, Tecnoscienza, pp. 739–785.
Matsuoka, H., Okada, H., 1989. Quantitative analysis of Quaternary nannoplankton in the subtropical northwestern Pacific Ocean. Mar. Micropaleontol. 14, 97–118.
Matsuzaki, K.M., Nishi, H., Suzuki, N., Cortese, G., Eynaud, F., Takashima, R., Kawate, Y., Sakai, T., 2014a. Paleoceanographic history of the Northwest Pacific Ocean over the past 740 kyr, discerned from radiolarian fauna. Palaeogeogr. Palaeoclimatol. Palaeoecol. 396, 26–40.
Matsuzaki, K.M., Suzuki, N., Nishi, H., Takashima, R., Kawate, Y., Sakaii, T., 2014b. Middle to late Pleistocene radiolarian biostratigraphy in the water-mixed region of the Kuroshio and Oyashio currents, northeastern margin of Japan (JAMSTEC Hole 902-C9001C). J. Micropalaeontol. 33, 205–222.
Matsuzaki, K.M., Suzuki, N., Nishi, H., Hayashi, H., Gyawali, B.R., Takashima, R., Ikehara, M., 2015. Early to Middle Pleistocene paleoceanographic history of southern Japan based on radiolarian data from IODP Exp. 314/315 Sites C0001 and C0002. Mar. Micropaleontol. 118, 17–33.
Mix, A.C., Pisias, N.G., Rugh, W., Wilson, J., Morey, A., Hagelberg, T.K., 1995. Benthic Foraminifer Stable Isotope Record from Site 849 (0–5 Ma): Local and Global Climate Changes.
Moore Jr., T.C., Skackleton, N.J., Pisias, N.G., 1993. Paleoceanography and the diachrony of radiolarian events in the eastern equatorial Pacific. Paleoceanography 8, 567–586. https://doi.org/10.1029/93PA01328.
Motoyama, I., Nishimura, A., 2005. Distribution of radiolarians in North Pacific surface sediments along the 175 E meridian. Paleontol. Res. 9, 95–117.
Nguyen, T.M.P., Petrizzo, M.R., Speijer, R.P., 2009. Experimental dissolution of a fossil foraminiferal assemblage (Paleocene–Eocene thermal Maximum, Dababiya, Egypt): Implications for paleoenvironmental reconstructions. Mar. Micropaleontol. 73, 241–258.
Norris, R.D., 1996. Symbiosis as an evolutionary innovation in the radiation of Paleocene planktic foraminifera. Paleobiology 22, 461–480.
Norris, R.D., 2000. Pelagic species diversity, biogeography, and evolution. Paleobiology 26, 236–258.
Okada, H., Bukry, D., 1980. Supplementary modification and introduction of code numbers to the low-latitude coccolith biostratigraphic zonation (Bukry, 1973; 1975). Mar. Micropaleontol. 5, 321–325. https://doi.org/10.1016/0377-8398(80)90016-X.
Paillard, D., Labeyrie, L., Yiou, P., 1996. Macintosh program performs time-series analysis. Eos. Trans. Am. Geophys. Union 77, 379.
Parker, W.C., Feldman, A., Arnold, A.J., 1999. Paleobiogeographic patterns in the morphologic diversification of the Neogene planktonic foraminifera. Palaeogeogr. Palaeoclimatol. Palaeoecol. 152, 1–14.
Petrick, B., Martínez-García, A., Auer, G., Reuning, L., Auderset, A., Deik, H., Takayanagi, H., De Vleeschouwer, D., Iryu, Y., Haug, G.H., 2019. Glacial indonesian throughflow weakening across the mid-pleistocene climatic transition. Sci. Rep. 9, 1–13.
Pujol, C., Duprat, J., 1983. Quaternary Planktonic Foraminifers of the Southwestern Atlantic (Rio-Grande rise) Deep-Sea Drilling Project Leg-72. Initial Rep. Deep Sea Drill. Proj. 72, 601–622.
Raffi, I., 2002. Revision of the early-middle Pleistocene calcareous nannofossil biochronology (1.75–0.85 Ma). Mar. Micropaleontol. 45, 25–55.
Raffi, I., Backman, J., 2022. The role of calcareous nannofossils in building age models for Cenozoic marine sediments: a review. Rend. Lincei. Sci. Fis. e Nat. 33, 25–38.
Raffi, I., Backman, J., Rio, D., Shackleton, N.J., 1993. Plio-Pleistocene Nannofossil Biostratigraphy and Calibration to Oxygen Isotope Stratigraphies from Deep Sea Drilling Project Site 607 and Ocean Drilling Program Site 677. Paleoceanography 8, 387–408. https://doi.org/10.1029/93PA00755.
Raffi, I., Backman, J., Fornaciari, E., Pälike, H., Rio, D., Lourens, L., Hilgen, F., 2006. A review of calcareous nannofossil astrobiochronology encompassing the past 25 million years. Quat. Sci. Rev. 25, 3113–3137.
Ramsey, C.B., 2009a. Dealing with outliers and offsets in radiocarbon dating. Radiocarbon 51, 1023–1045.
Ramsey, C.B., 2009b. Bayesian analysis of radiocarbon dates. Radiocarbon 51, 337–360.
Retailleau, S., Eynaud, F., Mary, Y., Abdallah, V., Schiebel, R., Howa, H., 2012. Canyon heads and river plumes: how might they influence neritic planktonic foraminifera communities in the SE Bay of Biscay? J. Foraminifer. Res. 42, 257–269.
Richardson, L.E., Middleton, J.F., Kyser, T.K., James, N.P., Opdyke, B.N., 2019. Shallow water masses and their connectivity along the southern Australian continental margin. Deep Sea Res. Part I Oceanogr. Res. Pap. 152, 103083.
Rio, D., Raffi, I., Villa, G., 1990. Pliocene-Pleistocene Calcareous Nannofossil Distribution Patterns in the Western Mediterranean, in: Proceedings of the Ocean Drilling Program. Scientific Results. Ocean Drilling Program College Station, TX, pp. 513–533.
Ruddiman, W.F., 2006. What is the timing of orbital-scale monsoon changes? Quat. Sci. Rev. 25, 657–658.
Sabba, M., Hanif, M., Mohibullah, M., Ullah, S., Ishaq, M., Ghani, M., 2022. Planktonic foraminiferal biostratigraphy and palaeobiogeography of the Albian–Turonian succession from the Sulaiman Range, Pakistan. Geol. J. https://doi.org/10.1002/gj.4660 in press.
Sato, T., Takayama, T., 1992. A stratigraphically significant new species of the calcareous nannofossil Reticulofenestra asanoi. Centen. Japanese Micropaleontol. 457, 460.
Sato, T., Kameo, K., Takayama, T., 1991. Coccolith biostratigraphy of the Arabian Sea. Proc. Ocean Drill. Program Sci. Results 117, 37–54.
Sato, T., Kameo, K., Mita, I., 1999. Validity of the latest Cenozoic calcareous nannofossil datums and its application to the tephrochronology. Earth Sci. (Chikyu Kagaku) 53, 265–274. https://doi.org/10.15080/agcjchikyukagaku.53.4_265.
Schiebel, R., Hemleben, C., 2017. Planktic Foraminifers in the Modern Ocean, 2nd ed. Springer.
Schiebel, R., Zeltner, A., Treppke, U.F., Waniek, J.J., Bollmann, J., Rixen, T., Hemleben, C., 2004. Distribution of diatoms, coccolithophores and planktic foraminifers along a trophic gradient during SW monsoon in the Arabian Sea. Mar. Micropaleontol. 51, 345–371.
Schloesser, F., 2014. A dynamical model for the Leeuwin Undercurrent. J. Phys. Oceanogr. 44, 1798–1810.
Schmuker, B., 2000. Recent planktic foraminifera in the Caribbean Sea: distribution, ecology and taphonomy. In: ETH Zurich. https://doi.org/10.3929/ethz-a-003887547.
Scotese, C.R., 2014. Atlas of Neogene Paleogeographic Maps (Mollweide Projection), Maps 1–7, volume 1, the Cenozoic, PALEOMAP Atlas for ArcGIS, PALEOMAP Project, Evanston, IL. Website www. Acad. Edu/11082185/AtlasofNeogenePaleogeographicMaps.
Spencer-Cervato, C., Thierstein, H.R., 1997. First appearance of Globorotalia truncatulinoides: cladogenesis and immigration. Mar. Micropaleontol. 30, 267–291.

Tagliaro, G., Fulthorpe, C., Watkins, D., Brumsack, H., Jovane, L., 2021. Southern Ocean carbonate dissolution paced by Antarctic Ice-Sheet expansion in the early Miocene. Glob. Planet. Chang. 202, 103510.
Tagliaro, G., Fulthorpe, C.S., Watkins, D.K., De Vleeschouwer, D., Brumsack, H., Bogus, K., Lavier, L.L., 2022. Late Miocene-Pliocene Vigorous Deep-Sea Circulation in the Southeast Indian Ocean: Paleoceanographic and Tectonic Implications. Paleoceanogr. Paleoclimatol. 37, e2021PA004303.
Takayama, T., Sato, T., 1987. Coccolith Biostratigraphy of the North Atlantic Ocean, Deep Sea Drilling Project Leg 94. In: Orlofsky, S. (Ed.), Initial Reports of the Deep Sea Drilling Project. U.S. Govt. Printing Office, Washington, pp. 651–702.
Tappan, H., Loeblich Jr., A.R., 1973. Evolution of the oceanic plankton. Earth-Science Rev. 9, 207–240.
Thierstein, H.R., Geitzenauer, K.R., Molfino, B., Shackleton, N.J., 1977. Global synchroneity of late Quaternary coccolith datum levels Validation by oxygen isotopes. Geology 5, 400–404.
Thompson, P.R., Bé, A.W.H., Duplessy, J.-C., Shackleton, N.J., 1979. Disappearance of pink-pigmented Globigerinoides ruber at 120,000 yr BP in the Indian and Pacific Oceans. Nature 280, 554–558.
Thunell, R.C., 1981. Cenozoic palaeotemperature changes and planktonic foraminiferal speciation. Nature 289, 670–672.
Tsandev, I., Slomp, C.P., Van Cappellen, P., 2008. Glacial-interglacial variations in marine phosphorus cycling: Implications for ocean productivity. Global Biogeochem 22.
Vats, N., Mishra, S., Singh, R.K., Gupta, A.K., Pandey, D.K., 2020. Paleoceanographic changes in the East China Sea during the last~ 400 kyr reconstructed using planktic foraminifera. Glob. Planet. Chang. 189, 103173.
Wade, B.S., Pearson, P.N., Berggren, W.A., Pälike, H., 2011. Review and revision of Cenozoic tropical planktonic foraminiferal biostratigraphy and calibration to the geomagnetic polarity and astronomical time scale. Earth-Science Rev. 104, 111–142.
Wei, K., Kennett, J.P., 1986. Taxonomic evolution of Neogene planktonic foraminifera and paleoceanographic relations. Paleoceanography 1, 67–84.
Wijeratne, S., Pattiaratchi, C., Proctor, R., 2018. Estimates of surface and subsurface boundary current transport around Australia. J. Geophys. Res. Ocean. 123, 3444–3466. https://doi.org/10.1029/2017JC013221.
Winter, D., Sjunneskog, C., Scherer, R., Maffioli, P., Riesselman, C., Harwood, D., 2012. Pliocene–Pleistocene diatom biostratigraphy of nearshore Antarctica from the AND-1B drillcore, McMurdo Sound. Glob. Planet. Chang. 96, 59–74.
Woo, M., Pattiaratchi, C., 2008. Hydrography and water masses off the western Australian coast. Deep Sea Res. Part I Oceanogr. Res. Pap 55, 1090–1104.
Young, J.R., 1998. Neogene nannofossils. In: Bown, P.R. (Ed.), Neogene Nannofossils. Kluwer Academic, pp. 225–266. https://doi.org/10.1007/978-94-011-4902-0_8.
Young, J.R., Bown, P.R., Lees, J.A., 2018. Nannotax3. International Nannoplankton Association.